

DESIGN OF AN OCTO-STRAIN SPECIMEN FOR BIAXIAL TENSION TESTING

Justin L. Milner and Thomas Gnäupel-Herold
National Institute of Standards and Technology,
NIST Center for Neutron Research
Gaithersburg, MD, USA

KEYWORDS

Sheet metal, Biaxial testing, Cruciform specimen, Octo-Strain specimen, Digital image correlation

ABSTRACT

A custom biaxial testing fixture was designed to evaluate a new specimen geometry for complex loading paths. Biaxial testing is commonly used to evaluate work-hardening behavior of sheet metal in biaxial tension to study the accumulation of plastic strains to determine the anisotropic yield loci. The current state-of-the-art specimen geometry that is used for biaxial testing is the cruciform specimen. Cruciform specimens are machined into a geometry that resembles a cross with four arms arranged at 90 degrees. However, this geometry is prone to premature failure and non-homogenous strain distribution within the gauge region. These problems persist even with the addition of complex features (*e.g.*, slits and multi-step pockets). Therefore, the primary goal of the new specimen geometry is to achieve a large and uniform strain field within the gauge region. One of the main problems of the cruciform specimen is the formation of stress concentration within the gauge region. Therefore, the proposed specimen geometry is comprised of four additional arms between the existing cruciform arms. This geometry is termed an ‘Octo-Strain’ specimen after the eight arms that are arranged in a 45-degree planar pattern. It is hypothesized that the additional arms will stabilize the stress concentrations and, thus, achieve increased failure strain and uniformity as compared to the cruciform geometry. This work focuses on the comparison of the cruciform specimen to the Octo-Strain specimen during balanced biaxial deformation of mild steel. It is found that the Octo-Strain specimen achieved twice the failure strain and increased strain uniformity within the gauge region as compared to the cruciform specimen.

INTRODUCTION

Biaxial testing is a method to determine material data that can be used for finite element modeling by deforming sheet metal material under complex strain paths. These methods include punch tests (*e.g.*, Marciniak and Nakazima) [1-3], bulge pressure tests [4-6], biaxial compression tests [7], and cruciform tests [8-10] to name a few. Each of these techniques has their advantages and disadvantages; such cons include the introduction of bending stresses and friction during the test, sample geometry issues, and measuring the stress-strain relationship. Cruciform testing eliminates the issues associated with the introduction of bending stresses and friction as it is an in-plane testing technique. The cruciform specimen geometry is derived from the standard uniaxial tensile test specimen, with the addition of a second loading direction resulting in a geometry that resembles two uniaxial specimens arranged perpendicular to each other (resembling a cross). The arms of the cruciform specimen are given a displacement that induces a biaxial force over the planar gauge area (at the intersection of the arms or center of the specimen). However, the cruciform specimen geometry tends to lead to premature failure and, thus, the failure strain limit of the material is not reached. This is primarily due to high-stress localization that occurs within the fillet area of the specimen near the radius (connecting the arms). Therefore, a radically new specimen geometry is considered to replace the cruciform specimen.

This new geometry is an eight-arm specimen arranged in a 45-degree planar pattern or, in other words, two cruciform specimens with a 45-degree relative offset. It is termed the Octo-Strain specimen due to its eight arms. This geometry was chosen to stabilize the stress localization seen to occur with the cruciform specimen geometry. It is also derived from the punch test specimen geometries which have a 360-degree clamping

force around the sample. More arms will approximate 360° of clamping. However, space requirements are the limiting factor for the arrangement of 2^n arms, where n is greater than 3. Similar to the cruciform specimen, a geometry with uniform thickness and arm width is insufficient for plastic deformation in the gauge region. Therefore, a reduction in thickness (recess/pocket) is required to further localize plastic deformation within the gauge region. Figure 1 displays a schematic of the Octo-Strain specimen geometry with key definitions of dimensions. This geometry follows the same necessities as the cruciform specimen in that a central recess (gauge region) of reduced cross-section is needed to localize plastic deformation. The criteria that the Octo-Strain specimen should satisfy is (1) Uniform strain distribution within the gauge region. (2) Large strains are achievable in the gauge region. (3) Failure should occur within the gauge region. (4) Adequate gauge area for stress and strain measurement. (5) And the specimen design should be simple and economical to manufacture.

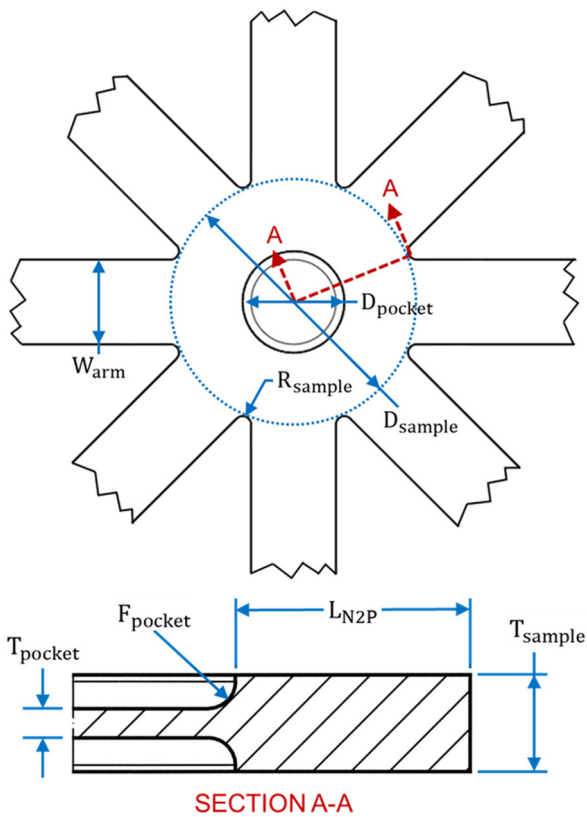


Figure 1: Schematic of an Octo-Strain specimen geometry and definitions of dimensions.

With a new Octo-Strain specimen geometry comes a new design of the biaxial testing system, the Octo-Strain electro-mechanical frame. Octo-Strain, shown in Figure 2, was custom designed to test the eight-arm samples under complex loading paths with in-situ stress and strain measurements via neutron diffraction and digital image correlation, respectively. This

loading frame has eight independently controlled actuators with a capacity of ± 15 kN and a stroke of ~ 30 mm. Each actuator can be controlled in displacement, load or strain control mode with the ability to switch between modes without unloading. Numerous strain paths can be achieved through varying the actuator velocities. The deformation of the samples is recorded using full-field digital image correlation (DIC), and this system can also be used for real-time strain control. Furthermore, in-situ neutron diffraction for stress measurement is intended during testing but is not used for the tests described in this paper. However, this capability leads to unique design criteria resulting in an “open” design to not obscure the neutron beam path and 360-degree rotation about the sample normal allowing for the determination of the planar stress tensor components.

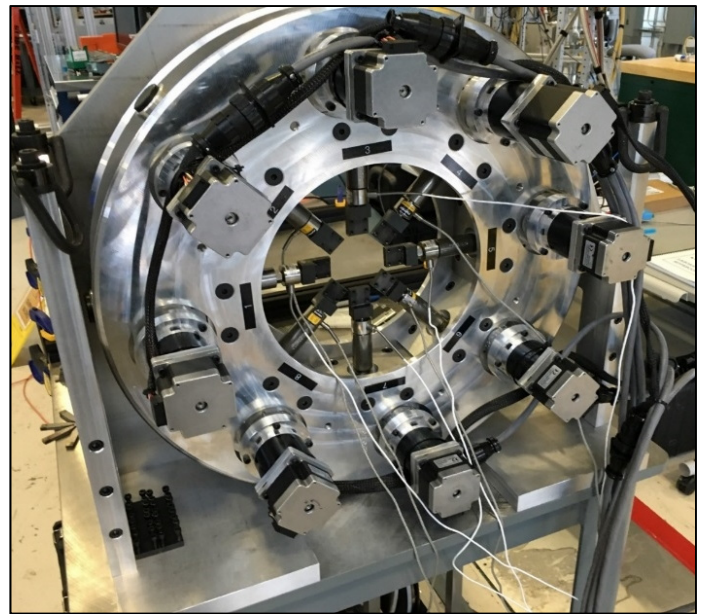


Figure 2: Photograph of the Octo-Strain biaxial loading device.

This work focuses on the comparison between the cruciform specimen geometry and the new Octo-Strain specimen geometry under balanced biaxial loading. Full-field strain mapping evaluates the performance of the specimen geometries tested via digital image correlation.

EXPERIMENTAL PROCEDURE

Experiments are conducted to evaluate the performance of the Octo-Strain specimen and compared to the cruciform specimen. The material used in this study is cold-rolled mild steel (AISI 1010) sheets received in a thickness of 3.31 ± 0.01 mm. All samples were waterjet cut along the outside profile, and the sample pocket was machined with a 1 mm corner radius end mill. A custom designed jig was created to position the samples, during the machining of the pocket, to ensure a centered pocket with respect to the sample. The experiments were performed with the Octo-Strain biaxial testing system (shown in Figure 2),

as described earlier. The specimens were tested under balanced biaxial deformation using load control to maintain a constant load ratio of one. The tests were conducted until the specimen fractured or when necking was observed within the arms. The strain evolution of the specimens was recorded with a full-field digital image correlation system.

To evaluate the samples equally, peak force was taken as a reference point for each test. The peak force was determined by taking the average of the load cell readings from the eight arms (four for the cruciform sample), then determining the maximum value. At peak force, a subset of the gauge region is analyzed to determine the average strain and strain homogeneity. The gauge region of the sample is defined as $D_{pocket} - 2 \times F_{pocket}$, which is the flat section of the sample pocket. The area used for determining strain and strain homogeneity is termed ‘gauge area’ and is defined as the area within a diameter equal to $0.3 \times D_{pocket}$. Furthermore, strain values along four line slices (two line slices for the cruciform geometry) connecting the sample’s radii was extracted and averaged into a single line slice (see Figure 3), to analyze the strain profile. The gauge area and line slice is schematically shown in Figure 3.

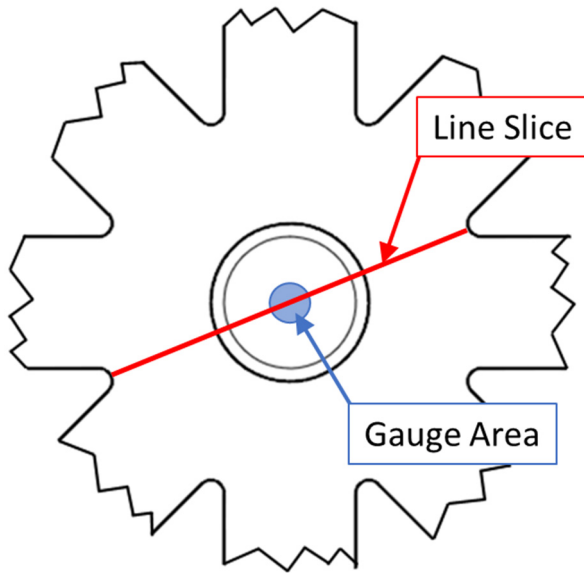


Figure 3: Schematic representation of the analyzed gauge region and line slice.

RESULTS AND DISCUSSION

To evaluate the performance of Octo-Strain specimen and compare it to the cruciform specimen without bias, geometries where chosen to compare the two best. Preliminary testing was conducted on the two specimen geometries, and it was determined that decreasing the thickness ratio, defined as the pocket thickness divided by the sample thickness ($t_{ratio} = t_{pocket}/t_{sample}$), increases the strain achieved in the gauge region regardless of other key parameters (*i.e.* pocket diameter).

Therefore, the thickness ratio of 0.25 was chosen for testing both specimen geometries, this corresponds to a $t_{sample} = 3.2 \text{ mm}$ and $t_{pocket} = 0.8 \text{ mm}$. Multiple sample radii (R_{sample}) were tested for both the specimen geometries and it was determined that a $R_{sample} = 12 \text{ mm}$ (cruciform) and a $R_{sample} = 1 \text{ mm}$ (Octo-Strain) provided the best results. These specimen geometries discussed in detail in this work are not considered optimal, as it may require more complex geometries of the specimen and/or gauge region. Therefore, in this work, only the pocket diameter (D_{pocket}) was evaluated experimentally to determine optimal performance, then the optimal specimen is chosen for further examination and comparison.

For the cruciform specimen, the D_{pocket} was varied between 15 mm and 18 mm at 1 mm intervals. These results are portrayed in Figure 4, displaying resultant pocket diameter versus effective strain at peak force. Decreasing the pocket diameter increases the strain achieved within the gauge region, until a drastic drop off in the strain level is noticed at a diameter of 15 mm. This reduction in strain is due to the increased sample material around the gauge region causing strain localization to occur in the arms of the specimen. This occurs around a D_{pocket} of 15 mm for the cruciform specimen with a R_{sample} of 12 mm, thus a D_{pocket} of 16 mm is near optimal for this geometry and selected for further discussion.

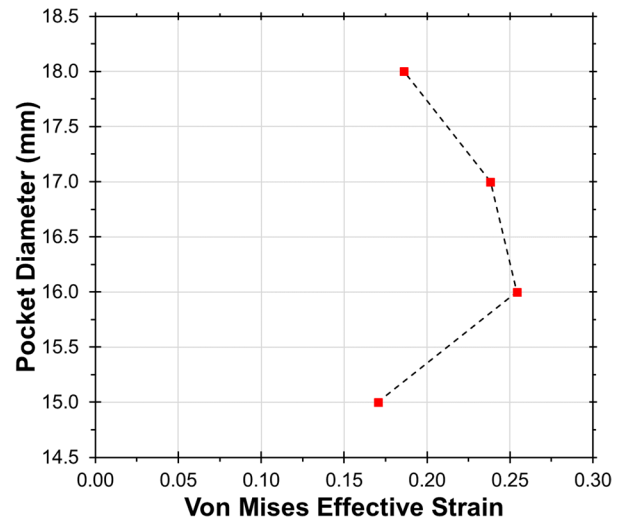


Figure 4: Pocket Diameter versus effective strain of cruciform sample geometry.

Figure 5 displays (a) average force per arm versus effective strain and (b) strain path of the cruciform specimen with a D_{pocket} of 16 mm. The horizontal and vertical dashed lines, within Figure 5, indicates peak force and corresponding effective strain. Peak force was recorded at $8.97 \pm 0.12 \text{ kN}$ occurring at an effective strain of 0.247 ± 0.007 . The horizontal and vertical dashed lines in Figure 5(b) represents the strain achieved in the x-direction (ϵ_{xx}) and y-direction (ϵ_{yy}) at peak force. The strain path is nearly ideal balanced biaxial where $\epsilon_{xx} = 0.123 \pm 0.008$ and

$\epsilon_{yy} = 0.123 \pm 0.006$ at peak force. Furthermore, the strain path remains balanced biaxial just prior to failure. It should be noted that the acquisition rate was changed mid-test from 1 frame per 2 seconds to 1 frame per 4 seconds without stopping deformation. This is most notable in Figure 5(b), where a slight pause is seen around a balanced strain of 0.11 and the data rate appears to slow thereafter. This change in the acquisition rate does not affect the test results.

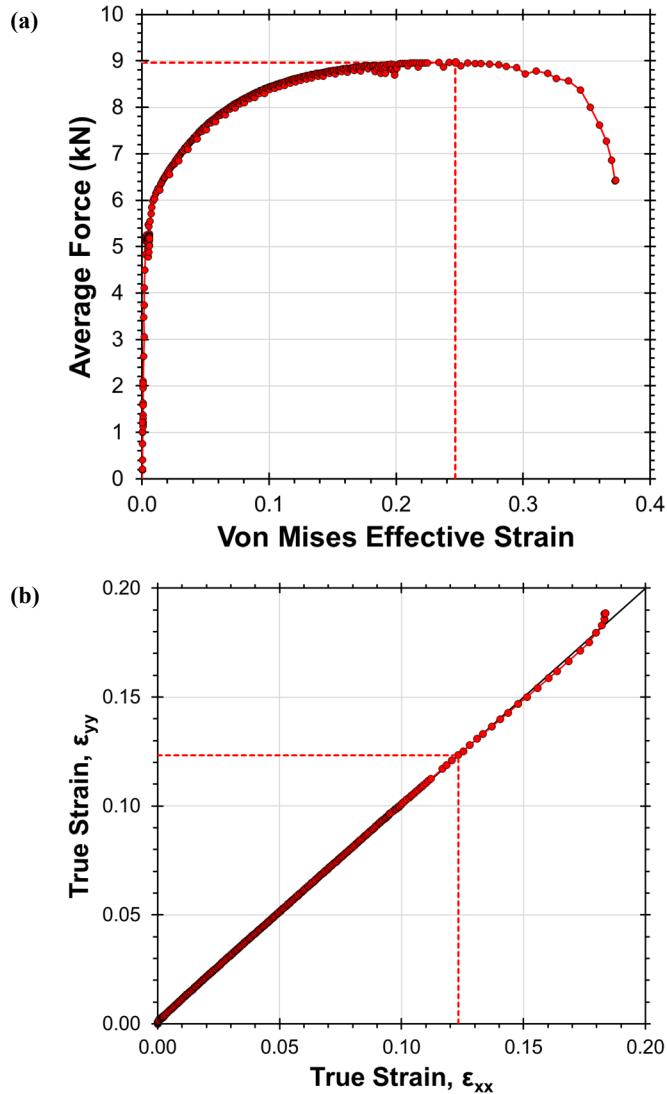


Figure 5: (a) average force versus effective strain and (b) strain path of the cruciform specimen with 16 mm pocket diameter

To further investigate the performance of the cruciform specimen geometry, the full-field strain data was examined for strain homogeneity and strain profile. Figure 6(a) displays the full-field strain map overlaid on the deformed sample at peak force. The strain is seen to localize near the pocket fillet at the location closest to the sample radius. This is more evident by the strain profile, shown in Figure 6(b), represented by the solid red line. This profile is derived from the line slice data and is plotted

based on the undeformed sample. The break in the strain profile data is where DIC is unable to determine strains due to geometry effects caused by the pocket fillet. The cruciform specimen exhibits a maximum effective strain of 0.47 near the pocket fillet, as compared to the minimum of 0.24 at the center of the gauge region. This significant variation of strain within the gauge region results in a less homogenous strain distribution. Analyzing the cruciform specimen results in an effective strain of 0.247 with a 0.007 standard deviation. This is represented graphically in Figure 6(b) where the blue lines depict the gauge area. The solid line signifies the mean and the dashed lines indicate the upper and lower bounds. The width of the lines also implies the diameter of the circular gauge area.

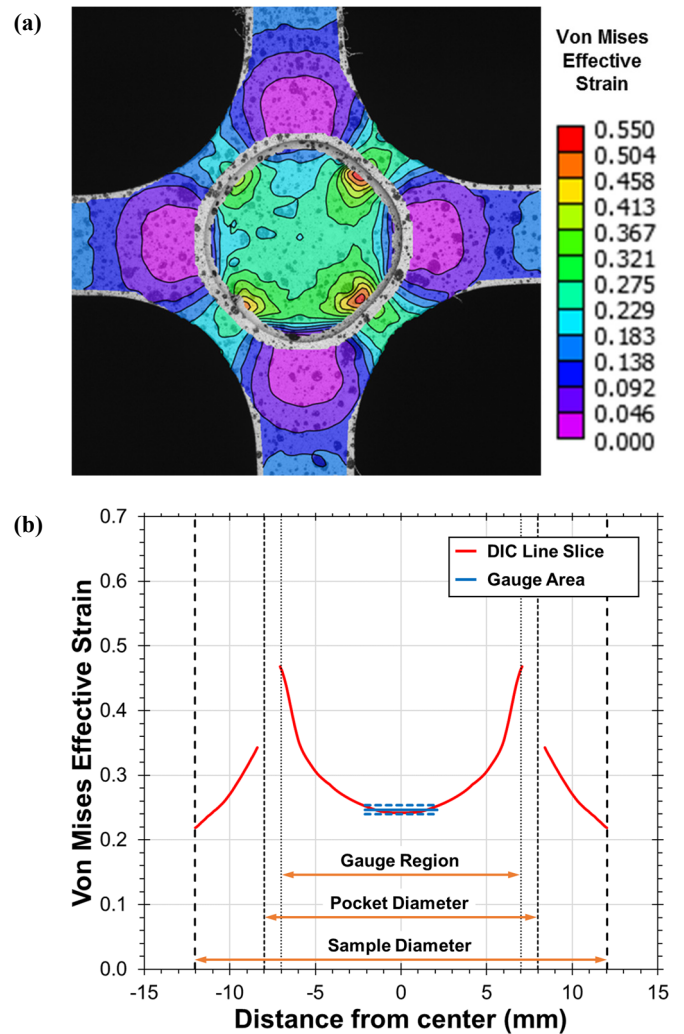


Figure 6: Cruciform sample showing (a) DIC measured von Mises effective strain (at peak force) overlaid on the image and (b) effective strain profile along line slice (red line) with average gauge area strain and variation (blue lines).

These results of the cruciform specimen compare favorably with the work of Creuziger et al. [11], where they determined an optimized cruciform geometry through FEA. Their optimized

specimen, of mild steel, resulted in an effective strain of 0.246 ± 0.011 determined at 90% of the strain at peak force and within a 25% gauge area. Using the same definitions as described in [11], the cruciform specimen with a pocket diameter of 16 mm, analyzed here, results in an effective strain of 0.227 ± 0.011 . In comparison, the cruciform geometry in this work achieved 0.019 less strain as compared to [11], corresponding to an 8% difference. Again, the cruciform geometry tested in this work is not considered optimized.

For the Octo-Strain specimen, the results of varying the pocket diameter is portrayed in Figure 7, where the D_{pocket} was varied between 10 mm and 14 mm with an interval of 1 mm while skipping 13 mm. These results exhibited a similar trend as observed with the cruciform specimen geometry, where decreasing the pocket diameter increases the strain achieved within the gauge region until a drastic drop is noticed. This drop occurs when strain localizes within the arms of the Octo-Strain specimen, around a pocket diameter of 10 mm. The Octo-Strain specimen with a pocket diameter of 12 mm slightly outperformed the specimen with 11 mm pocket diameter. It is assumed that the optimal geometry of the Octo-Strain specimen is near the 11 mm pocket diameter. This is supported by FE modeling that will be discussed in detail in a later paper. This occurrence may be due to slight thickness variation within the gauge region. Therefore, the Octo-Strain specimen with a pocket diameter of 12 mm is selected for further examination and comparison.

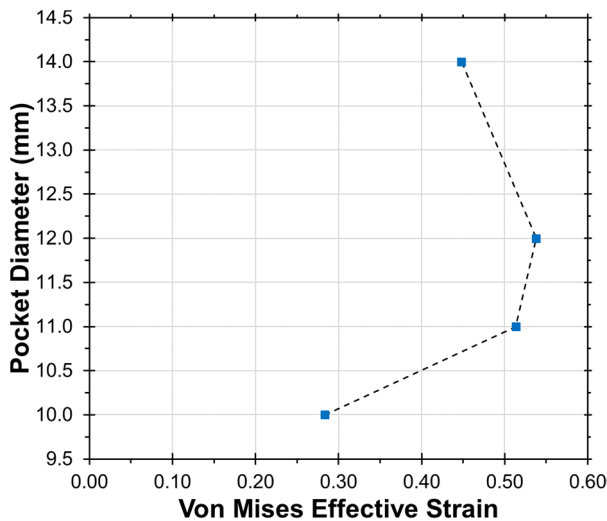


Figure 7: Pocket Diameter versus effective strain of Octo-Strain sample geometry.

The average force per arm versus effective strain and the resultant strain path for the Octo-Strain specimen with a pocket diameter of 12 mm are portrayed in Figure 8, along with the results of the cruciform specimen in gray for reference. The average peak force per arm is 9.07 ± 0.12 kN, which is similar to the cruciform specimen. At peak force, the effective strain was 0.538 ± 0.003 , which is over twice the strain achieved by the

cruciform specimen. This is further realized by the strain path where $\epsilon_{xx} = 0.262 \pm 0.002$ and $\epsilon_{yy} = 0.275 \pm 0.002$ at peak force. The strain path of the Octo-Strain specimen veers off balanced biaxial at higher strains. This is due to the load control regime that was chosen for these tests, and if strain control was employed this deviation would not arise. The load deviation throughout the test was 121 N, even up to failure.

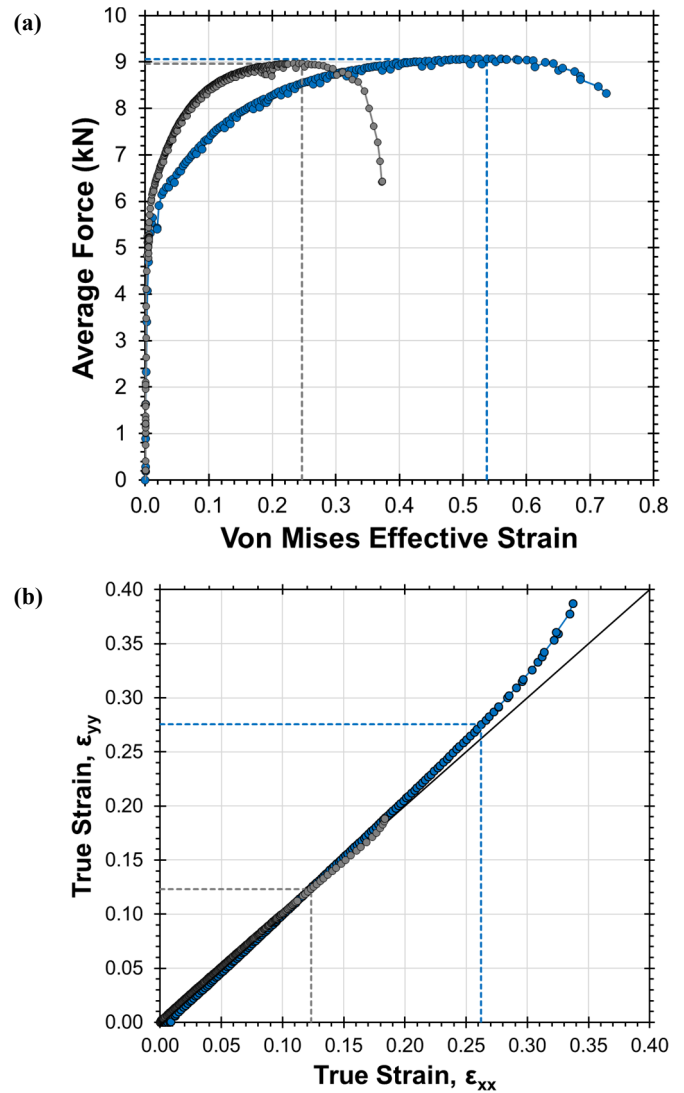


Figure 8: (a) average force versus effective strain and (b) strain path of the Octo-Strain specimen with 12 mm pocket diameter. The cruciform specimen with 16 mm pocket diameter is also shown in gray for reference.

To further compare the Octo-Strain specimen with the cruciform specimen, the full-field DIC data is examined and displayed in Figure 9. The maximum effective strain of 0.57 is seen to occur at the samples' radii, as observed in Figure 9(a). Moreover, the gauge region of the Octo-Strain specimen has a more homogeneous strain field. This is more evident when examining the strain profile, shown in Figure 9(b), represented

by the solid red line. A large strain gradient occurs from the sample radius to the pocket diameter by a factor of three. Nevertheless, the strain gradient within the gauge region is minor in comparison, with a rather uniform strain field in the center of the gauge region. This provides a sufficient area (approximately 6 mm in diameter) for measuring stress, via neutron diffraction, with minimal error due to strain uncertainty. Analyzing the Octo-Strain specimen results in a measured effective strain of 0.538 ± 0.003 , graphically portrayed in Figure 9. The gauge area is depicted by the blue lines, where the solid line indicates the average effective strain and the dashed lines represent the variation.

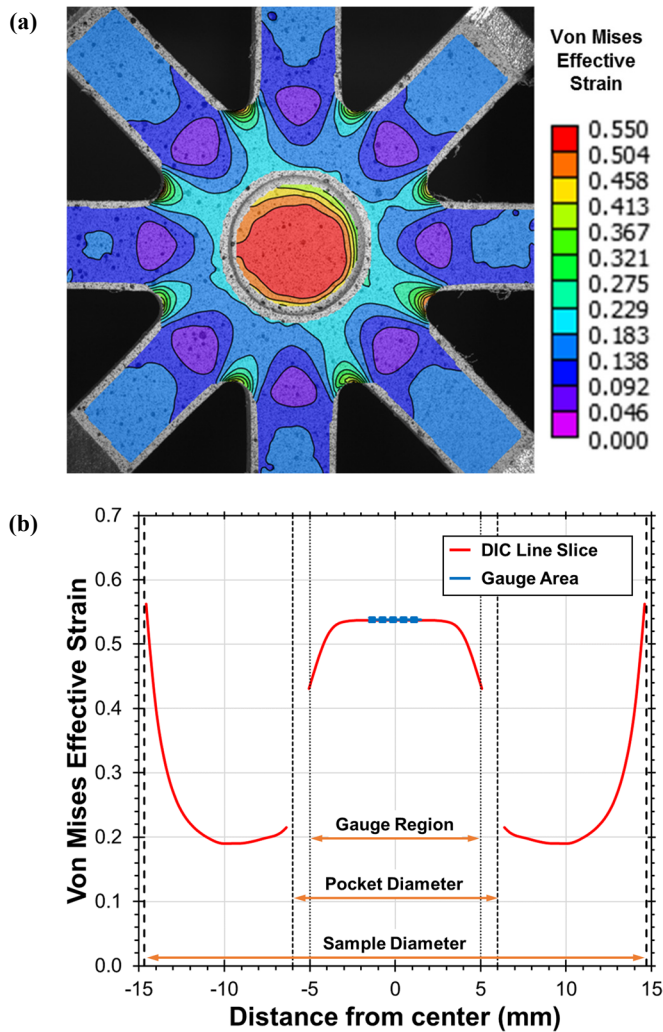


Figure 9: Octo-Strain sample showing (a) DIC measured von Mises effective strain (at peak force) overlaid on the image and (b) effective strain profile along line slice (red line) with average gauge area strain and variation (blue lines).

SUMMARY AND CONCLUSIONS

The findings presented here are the first glimpse into the design and performance of the Octo-Strain specimen, a novel geometry for biaxial testing. When comparing the two specimen geometries, the Octo-Strain geometry outperforms the cruciform. In terms of strain at peak force, the cruciform reached an effective strain of 0.247, as compared to 0.538 for the Octo-Strain specimen. This corresponds to a twofold increase in strain achieved for the Octo-Strain specimen. Furthermore, the strain field within the gauge region is more homogeneous for the Octo-Strain specimen, leading to more accurate measurements. This homogeneity increase is due to a smaller strain gradient within the gauge region as compared to the cruciform specimen. Future work will consist of FEA modeling to determine an optimized Octo-Strain geometry and testing of various materials.

REFERENCES

- [1] Z. Marciniak and K. Kuczyński, "Limit Strains in the Processes of Stretch-Forming Sheet Metal," *International Journal of Mechanical Sciences*, vol. 9, pp. 609-620, 1967.
- [2] K. Nakazima, T. Kikuma, and K. Hasuka, "Study on the Formability of Steel Sheets," *Yawata Technical Report*, vol. 264, pp. 8517-8530, 1968.
- [3] S. P. Keeler and W. A. Backofen, "Plastic Instability and Fracture in Sheets Stretched Over Rigid Punches," *ASM Trans Q*, vol. 56, pp. 25-48, 1963.
- [4] A. Ranta-Eskola, "Use of the Hydraulic Bulge Test in Biaxial Tensile Testing," *International Journal of Mechanical Sciences*, vol. 21, pp. 457-465, 1979.
- [5] D. Rees, "Plastic Flow in the Elliptical Bulge Test," *International Journal of Mechanical Sciences*, vol. 37, pp. 373-389, 1995.
- [6] J. Liu, M. Ahmetoglu, and T. Altan, "Evaluation of Sheet Metal Formability, Viscous Pressure Forming (VPF) Dome Test," *Journal of Materials Processing Technology*, vol. 98, pp. 1-6, 2000.
- [7] Y. Tozawa and M. Nakamura, "New Method for Testing Sheet Under Biaxial Compression," *Journal of Japan Society for Technology of Plasticity*, vol. 13, pp. 538-541, 1972.
- [8] E. Shiratori and K. Ikegami, "Experimental Study of the Subsequent Yield Surface by Using Cross-Shaped Specimens," *Journal of the Mechanics and Physics of Solids*, vol. 16, pp. 373-394, 1968.
- [9] S. Demmerle and J. P. Boehler, "Optimal Design of Biaxial Tensile Cruciform Specimens," *Journal of the Mechanics and Physics of Solids*, vol. 41, pp. 143-181, 1993.
- [10] W. Müller and K. Pöhlandt, "New Experiments for Determining Yield Loci of Sheet Metal," *Journal of Materials Processing Technology*, vol. 60, pp. 643-648, 1996.
- [11] A. Creuziger, M. A. Iadicola, T. Foecke, E. Rust, and D. Banerjee, "Insights into Cruciform Sample Design," *JOM*, vol. 69, pp. 902-906, 2017.